

Monte Carlo Investigations of a Gay–Berne Liquid Crystal

Roberto Berardi, Andrew P. J. Emerson† and Claudio Zannoni*

Dipartimento di Chimica Fisica ed Inorganica, Università, Viale Risorgimento 4, 40136 Bologna, Italy

We report extensive Monte Carlo simulations of two systems with 512 and 1000 particles interacting with a Gay–Berne potential with strength parameters ($\mu = 1$, $\nu = 3$) that enhance the side-by-side and end-to-end interactions between the particles. We show that the system has a smectic, nematic and isotropic phase and we calculate the order parameters $\langle P_2 \rangle$, $\langle P_4 \rangle$, the intermolecular vector distribution and other relevant observables as a function of temperature at a scaled density $\rho^* = 0.30$.

1. Introduction

Computer simulations of liquid crystals, although not nearly as abundant as simulations of ordinary liquids have started to become an important way of studying this fascinating category of fluids.¹ A number of simulations have appeared involving simple lattice models,^{2,3} hard ellipsoids and spherocylinders,^{4–6} anisotropic Lennard–Jones,⁷ Berne–Pechukas–Kushick^{8–10} and more recently Gay–Berne^{11–18} models. All of these simulations, although based on models of very different complexity and, possibly, of realism, rely on approximating each particle with one anisotropic object or interaction centre. A limited number of more realistic multi-centre approximations have also appeared,^{19–21} even though with a relatively small number of molecules. These kinds of simulations are important for looking at the detailed environment around a molecule but are probably not yet completely ripe for looking at phase transition and collective properties, where the requirement of large samples calls for simpler models.

The Gay–Berne (GB) model¹¹ is a sort of anisotropic Lennard–Jones potential that is rapidly becoming a prototype for simulations of liquid crystals.^{11–18} The potential has an attractive and repulsive part decreasing with separation r as r^{-6} and r^{-12} but with a rather complex form (*cf.* Section 1.1) that depends on the particle orientations as well as the intermolecular vector. The form of the Gay–Berne potential employed in most studies^{11–18} is a modified version of the gaussian overlap potential of Berne–Pechukas–Kushick^{8,9} that allows for a change in well depth and width when the orientation of the molecules, with respect to the intermolecular vector, changes.²²

The main characteristic of liquid crystals, and what makes them particularly difficult to study and simulate, is the existence of orientational and possibly positional order and the presence of transitions between phases where some of these order parameters vanish. A transition of particular importance is the nematic–isotropic one, where the orientational order goes to zero. This transition is experimentally of a weak first-order character and presents strong pretransitional effects.²³ While rather detailed studies of this orientational transition^{3,24} and other applications [see, *e.g.*, ref. 25, 26] have appeared and continue to appear for lattice models, most of the studies on the more complex systems with translational freedom have concentrated on proving the existence of one or more ordered phases and in sketching a phase diagram.^{12–18} The number of particles employed in these various studies is also necessarily rather different. Thus lattice models have comprised systems of up to a few tens of thousand particles, while simulations of particles with trans-

lational freedom have involved a number of particles, N , ranging from 108 and 168,¹⁰ to 256,^{13,14,16} to 500 and, in a limited number of runs, to 800.¹⁴

In this paper we wish to examine two systems of $N = 512$ and $N = 1000$ Gay–Berne particles with a parameterization to be discussed in some detail in the next section. We choose a certain density and perform heating and cooling temperature scans in rather small increments, to start and examine the phase transitions in some detail, at least as far as it is allowed by the sample size available. We also calculate second-rank and fourth-rank order parameters and the distribution of intermolecular vector as a function of temperature. We believe this to be important if comparison with approximate analytical theories has to be performed. A comparison is also provided between the parameterization employed here and that of various previous studies.^{11–17}

1.1 The Gay–Berne Potential

The anisotropic interaction between two particles i and j , which we can think as ellipsoids of revolution, with orientations given by unit vectors \mathbf{u}_i and \mathbf{u}_j and with centres separated by the intermolecular vector \mathbf{r} can be written according to the GB model as:¹¹

$$U_{\text{GB}} \equiv U(\mathbf{u}_i, \mathbf{u}_j, \mathbf{r}) = 4\epsilon(\mathbf{u}_i, \mathbf{u}_j, \hat{\mathbf{r}}) \left\{ \left[\frac{\sigma_s}{r - \sigma(\mathbf{u}_i, \mathbf{u}_j, \hat{\mathbf{r}}) + \sigma_s} \right]^{12} - \left[\frac{\sigma_s}{r - \sigma(\mathbf{u}_i, \mathbf{u}_j, \hat{\mathbf{r}}) + \sigma_s} \right]^6 \right\} \quad (1)$$

where $\hat{\mathbf{r}}$ is a unit vector along the intermolecular vector. The parameterization of the potential is rather complex but basically it can be related to shape and attractive energy anisotropy. The information about the shape of the particles is contained in the orientation dependent range parameter σ :

$$\sigma(\mathbf{u}_i, \mathbf{u}_j, \hat{\mathbf{r}}) = \sigma_s \left\{ 1 - \frac{\chi}{2} \left[\frac{(\mathbf{u}_i \cdot \hat{\mathbf{r}} + \mathbf{u}_j \cdot \hat{\mathbf{r}})^2}{1 + \chi(\mathbf{u}_i \cdot \mathbf{u}_j)} + \frac{(\mathbf{u}_i \cdot \hat{\mathbf{r}} - \mathbf{u}_j \cdot \hat{\mathbf{r}})^2}{1 - \chi(\mathbf{u}_i \cdot \mathbf{u}_j)} \right] \right\}^{-1/2} \quad (2)$$

where χ is determined by the shape anisotropy, $\kappa \equiv \sigma_e/\sigma_s$ of the particles:

$$\chi = \frac{\kappa^2 - 1}{\kappa^2 + 1} \quad (3)$$

Here σ_e , σ_s are size parameters reflecting the length and breadth of the particles. More precisely σ_e and σ_s are the separations at which the attractive and repulsive terms in the potential cancel when the molecules are in the end-to-end and side-by-side configuration.

† Present address: Department of Chemistry, The University, Southampton, UK SO9 5NH.

Table 1 Strength of interaction function $\varepsilon(\mathbf{u}_i, \mathbf{u}_j, \hat{\mathbf{r}})$ for selected intermolecular configurations

configuration	$\varepsilon(\mathbf{u}_i, \mathbf{u}_j, \hat{\mathbf{r}})/\varepsilon_0$	μ, ν	
		2, 1	1, 3
ee	$(1/\kappa')(1 - \chi^2)^{-\nu/2}$	1/3	25/27
ss	$(1 - \chi^2)^{-\nu/2}$	5/3	125/27
×	1	1	1
T	$[2/(\kappa'^{1/\mu} + 1)]^\mu$	$[4/(5^{1/2} + 1)^2]$	1/3

Here $\kappa \equiv \sigma_e/\sigma_s$ and $\kappa' \equiv \varepsilon_s/\varepsilon_e$. The last two columns correspond to different choices of (μ, ν) while keeping $\kappa = 3, \kappa' = 5, \varepsilon_0 = 1$.

The energy term in eqn. (1) can be written as proposed in ref. 11

$$\varepsilon(\mathbf{u}_i, \mathbf{u}_j, \hat{\mathbf{r}}) = \varepsilon_0 e'^{\mu}(\mathbf{u}_i, \mathbf{u}_j, \hat{\mathbf{r}}) \varepsilon^{\nu}(\mathbf{u}_i, \mathbf{u}_j) \quad (4)$$

where

$$\varepsilon(\mathbf{u}_i, \mathbf{u}_j) = [1 - \chi^2(\mathbf{u}_i \cdot \mathbf{u}_j)^2]^{-1/2} \quad (5)$$

and

$$\varepsilon'(\mathbf{u}_i, \mathbf{u}_j, \hat{\mathbf{r}}) = 1 - \frac{\chi'}{2} \left[\frac{(\mathbf{u}_i \cdot \hat{\mathbf{r}} + \mathbf{u}_j \cdot \hat{\mathbf{r}})^2}{1 + \chi'(\mathbf{u}_i \cdot \mathbf{u}_j)} + \frac{(\mathbf{u}_i \cdot \hat{\mathbf{r}} - \mathbf{u}_j \cdot \hat{\mathbf{r}})^2}{1 - \chi'(\mathbf{u}_i \cdot \mathbf{u}_j)} \right] \quad (6)$$

The parameter χ' reflects the anisotropy in the attractive forces,

$$\chi' = \frac{\kappa'^{1/\mu} - 1}{\kappa'^{1/\mu} + 1} \quad (7)$$

where κ' is the anisotropy ratio: $\kappa' = \varepsilon_s/\varepsilon_e$ and $\varepsilon_e, \varepsilon_s$ are the well depths for the end-to-end and side-by-side configurations.

The significance of the parameters and the effect of changing them can be made more apparent when considering selected orientations,¹³ as we do in Table 1.

The parameters $\kappa = 3, \kappa' = 5, \mu = 2, \nu = 1$ were considered in the molecular dynamics simulation works of Adams *et al.*,¹² Emsley *et al.*,¹⁶ de Miguel *et al.*¹⁵ and a full phase diagram study was obtained by Chalam *et al.*¹⁴ Another set of parameters, with $\kappa = 3, \kappa' = 5, \mu = 1, \nu = 2$ was studied by Luckhurst *et al.*¹³ where the existence of smectic, nematic and isotropic phases was clearly demonstrated, while the behav-

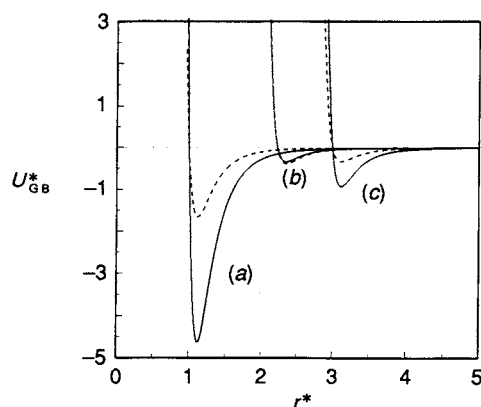


Fig. 1 GB potential $U_{GB}^* \equiv U_{GB}/\varepsilon_0$ corresponding to parameterizations $\mu = 1, \nu = 3$ (continuous line) and $\mu = 2, \nu = 1$ (dashed line) and $\kappa = 3, \kappa' = 5$ shown as a function of scaled intermolecular separation r^* , $r^* \equiv r/\sigma_s$, at three orientations. (a) side-by-side (ss), (b) tee (T) and (c) end-to-end (ee).

our inside the phases was not studied in detail. The systems studied have varied in size between $N = 256^{13,16}$ and 500^{14} particles.

In this paper we report rather extensive canonical ensemble Monte Carlo results for particles interacting with the $\mu = 1, \nu = 3$ GB potential.¹¹ We have found this modified interaction useful in a separate study of model GB droplets.²⁷ As far as we know this represents the first detailed study of the bulk behaviour of the GB potential using parameters different to those proposed by Gay and Berne.¹¹

The use of these modified parameters has the effect of lowering the well depths of the end-to-end and side-by-side configurations (see Table 1 and Fig. 1). On the other hand, the shape and well-depth anisotropy of the particles remain the same and we might wonder if differences in phase behaviour just consist of a scaling of the transition temperatures.

We test in particular if the behaviour of the GB potential for various choices of coefficients is universal. In other words we wish to check if the order parameters and, in general, the thermodynamic observables at the same reduced temperature T/T_{NI} are the same or not.

2. Simulation Results and Discussion

We have chosen GB particles with length to breadth ratio $\kappa \equiv \sigma_e/\sigma_s = 3$ and strength parameters $\kappa' \equiv \varepsilon_s/\varepsilon_e = 5, \mu = 1, \nu = 3$. Monte Carlo simulations in the canonical (NVT) ensemble were performed on systems of $N = 512$ and $N = 1000$ particles interacting *via* the modified GB potential described above and with the usual cubic periodic boundary conditions. The scaled density ρ^* ($\rho^* \equiv N\sigma_s^3/V$) was chosen to be 0.30 and the system was studied as a function of scaled temperature T^* , with $T^* \equiv \kappa T/\varepsilon_0$. Trial orientations of the particles were generated with the Barker–Watts technique²⁸ and the maximum angular and positional displacements were adjusted to give an acceptance ratio close to 0.5. Typical angular displacements compatible with this acceptance ratio were found to be *ca.* 15°. Adequate evolution of the system was achieved with this acceptance ratio.

To reduce the computational time a spherical cutoff of $4.0\sigma_s$ was employed in conjunction with a Verlet neighbour list.²⁹ It was found that with a list radius of $4.8\sigma_s$ the program was significantly (1.5 times) faster with respect to a calculation with the same cutoff but without the neighbour list. Neighbour list update was typically performed every 5–6 cycles (a cycle being a set of N attempted moves). Even with these precautions the computations are fairly heavy. For the $N = 1000$ particle systems the generation of 1000 cycles takes about 1 h on a Hewlett–Packard RISC workstation HP720.

The simulations for the $N = 512$ particles system were started from an initial configuration constructed from perfectly aligned particles positioned on a simple cubic lattice. The system was melted at a scaled temperature of $T^* = 5.0$ until isotropic, as identified by the value of $\langle P_2 \rangle$ calculated from diagonalization of the molecular \mathbf{Q} tensor.³⁰ A series of cooling runs were then performed with the starting configuration for each state point being taken from the simulation at the previous temperature. On average 10–20 000 cycles were used for equilibration and 10 000 cycles for the production stages but near phase transitions considerably longer runs were necessary (*cf.* Table 2).

The $N = 1000$ system was started from an isotropic configuration at $T^* = 4.0$ prepared, as before by melting a well ordered system at $T^* = 2.0$. Cooling runs were then typically performed in cascade, with some prolonged runs continued as judged necessary afterwards. Runs at temperatures higher than $T^* = 4.0$ were produced in a heating sequence. More heating and cooling runs were performed as will be described

later. Data referring to these two sequences will be marked with appropriate superscripts (c and h) when necessary in what follows. This large system required very long equilibration and production runs. We used at least 20 000 cycles for equilibration and 40 000 cycles for production. However, near the phase transitions considerably longer runs were necessary. In practice we went to more than 500 000 cycles near the nematic–isotropic (both for cooling and heating runs) and 130 000 near the nematic–smectic transition. In Fig. 2 we see some evolution diagrams that illustrate the need for these long runs. While the simulation equilibrates fairly quickly far from a phase change, *e.g.* here at $T^* = 2.00$, $T^* = 2.80$, we see a very persistent fluctuation near the transition ($T^* = 3.55$ and $T^* = 3.60$), that could produce quite misleading results if the production run was truncated after some thousand or tens of thousand cycles. The long fluctuation seemingly corresponds to the configurational bottleneck between isotropic and nematic phase and the fact that at a first-order transition both phases have, in principle, the same probability of occurrence. We notice that this phenomenon, well known in lattice-model studies³ is not always considered when dealing with models with translational freedom.

A summary of the results of the simulations for the $N = 512$ and $N = 1000$ systems are given in Tables 2 and 3. The reported errors were calculated as described in ref. 3. We shall now consider in detail the information obtained for the thermodynamics and the structure of the systems.

2.1 Thermodynamics

The variation of scaled internal energy $\langle U^* \rangle \equiv \langle U \rangle / \epsilon_0$ referred to one particle for the systems of $N = 512$ and $N = 1000$ particles with temperature is shown in Fig. 3. We see that the energy curve presents more than one change of slope. The highest temperature change of slope occurs around $T^* = 3.55$. We shall demonstrate later that this change of slope can be identified with the nematic–isotropic (NI) transition of the system. For the $N = 1000$ system we report results for a cooling sequence, with simulations started from an isotropic system and cooling down (∇) or *vice versa* continued from a set of simulations started on the cold side (Δ). As we can see hardly any hysteresis is apparent. This

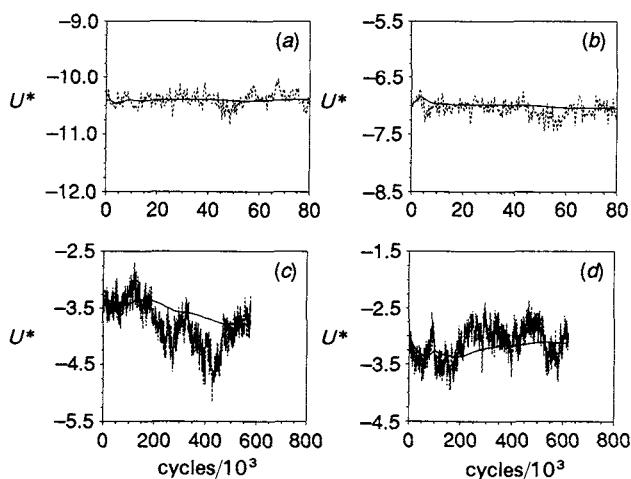


Fig. 2 Evolution charts of the scaled energy U^* with production cycles at scaled temperatures $T^* =$ (a) 2.00^b, (b) 2.80^b, (c) 3.55^c and (d) 3.60^c for the $N = 1000$ system. We also show the evolution of the cumulative average $\langle U^* \rangle$ (continuous line). Notice the different scales for the various scaled temperatures.

Table 2 Average scaled energy $\langle U^* \rangle$ and order parameter $\langle P_2 \rangle$ obtained from the production runs of the $N = 512$ simulations

T^*	$n_{\text{eq}}/10^3$	$\langle U^* \rangle$	$\langle P_2 \rangle$
1.90	5	-12.205 ± 0.014	0.952 ± 0.001
2.00	16	-11.851 ± 0.021	0.947 ± 0.001
2.20	20	-10.124 ± 0.025	0.922 ± 0.001
2.40	20	-8.342 ± 0.035	0.870 ± 0.004
2.60	10	-7.665 ± 0.035	0.844 ± 0.001
2.80	10	-7.147 ± 0.043	0.821 ± 0.004
3.00	10	-6.596 ± 0.034	0.788 ± 0.003
3.20	20	-5.986 ± 0.042	0.757 ± 0.005
3.40	70	-4.914 ± 0.042	0.645 ± 0.006
3.50	90	-4.803 ± 0.032	0.640 ± 0.005
3.55	20	-2.644 ± 0.013	0.133 ± 0.005
3.60	10	-2.473 ± 0.032	0.065 ± 0.004
3.80	15	-2.282 ± 0.019	0.083 ± 0.008
4.00	10	-2.055 ± 0.028	0.068 ± 0.006
5.00	10	-0.843 ± 0.020	0.091 ± 0.005

The column marked n_{eq} refers to the number of equilibration cycles employed for each scaled temperature. The production runs consisted in all cases of $n_{\text{prod}} = 10^4$ cycles.

seems to be at variance with the observations of Chalam *et al.*¹⁴ where large differences were found on the heating and cooling cycles of their molecular dynamics simulation on 500 GB particles with $\mu = 2$, $\nu = 1$ at a higher density, $\rho^* = 0.32$. In any case the fact that here the two branches match very well outside the small transition region indicates that the system is satisfactorily equilibrated.

The heat capacity of the system has been calculated as in ref. 3 by differentiating the energy with respect to temperature and is shown in Fig. 4 for the 512 and 1000 particles samples.

We notice at once the sharp peak of the isotropic transition and a lower, very broad one. The low-temperature hump seems to be the superposition of at least two peaks that could tentatively be associated with a crystal–smectic and smectic–nematic transition, while the possibility of a smectic–smectic phase change in between cannot be ruled out. The low temperature value of C_V^* , 2.7, is not too far from the one expected from a collection of harmonic oscillators–librators.

As far as the change with sample size is concerned, we can only really compare the high temperature NI anomaly. In this case the larger system presents a sharper and higher peak and an asymmetric shape, with a faster descent on the ‘hot’ side. This behaviour is consistent with a first-order transition. However, we should point out that the average values near the transition present extremely large fluctuations as the

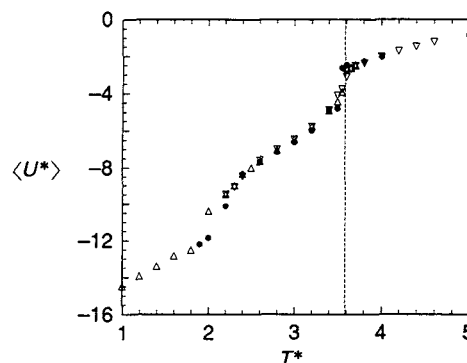


Fig. 3 Average scaled energy $\langle U^* \rangle$ as a function of scaled temperature T^* . We show results for the $N = 1000$ system in a cooling (∇) and heating (Δ) stage and results for the $N = 512$ system (\bullet). The vertical dashed line indicates the nematic–isotropic transition.

Table 3 Results for the $N = 1000$ simulations obtained from the n_{prod} production runs (in cycles) after n_{eq} equilibration cycles

T^*	$n_{\text{prod}}/10^3$	$n_{\text{eq}}/10^3$	$\langle U^* \rangle$	$\langle P_2 \rangle$	$\langle P_4 \rangle$
1.00 ^h	20	20	-14.480 ± 0.053	0.979 ± 0.001	0.932 ± 0.003
1.20 ^h	12	20	-13.934 ± 0.058	0.973 ± 0.001	0.915 ± 0.004
1.40 ^h	63	20	-13.389 ± 0.075	0.967 ± 0.002	0.896 ± 0.005
1.60 ^h	74	20	-12.839 ± 0.083	0.960 ± 0.002	0.874 ± 0.007
1.80 ^h	80	40	-12.524 ± 0.233	0.955 ± 0.004	0.860 ± 0.011
2.00 ^h	80	20	-10.394 ± 0.127	0.920 ± 0.004	0.761 ± 0.011
2.20 ^h	100	20	-9.472 ± 0.153	0.899 ± 0.005	0.709 ± 0.013
2.20 ^c	40	20	-9.478 ± 0.138	0.901 ± 0.005	0.712 ± 0.012
2.30 ^h	132	20	-8.988 ± 0.153	0.887 ± 0.006	0.680 ± 0.015
2.30 ^c	40	20	-9.077 ± 0.143	0.891 ± 0.006	0.688 ± 0.014
2.40 ^h	120	20	-8.340 ± 0.159	0.867 ± 0.008	0.637 ± 0.018
2.40 ^c	40	20	-8.475 ± 0.166	0.871 ± 0.008	0.643 ± 0.019
2.50 ^h	105	20	-8.001 ± 0.131	0.853 ± 0.008	0.604 ± 0.018
2.60 ^h	120	20	-7.648 ± 0.147	0.836 ± 0.011	0.570 ± 0.022
2.60 ^c	20	20	-7.584 ± 0.156	0.833 ± 0.010	0.564 ± 0.021
2.80 ^h	80	20	-7.040 ± 0.147	0.806 ± 0.012	0.517 ± 0.023
2.80 ^c	20	20	-6.987 ± 0.181	0.799 ± 0.017	0.508 ± 0.031
3.00 ^h	80	20	-6.447 ± 0.172	0.769 ± 0.016	0.458 ± 0.025
3.00 ^c	20	20	-6.451 ± 0.149	0.774 ± 0.009	0.466 ± 0.018
3.20 ^h	80	20	-5.765 ± 0.176	0.717 ± 0.018	0.385 ± 0.025
3.20 ^c	40	20	-5.796 ± 0.158	0.722 ± 0.013	0.391 ± 0.019
3.40 ^h	135	20	-4.918 ± 0.215	0.634 ± 0.028	0.293 ± 0.033
3.40 ^c	100	20	-4.888 ± 0.210	0.626 ± 0.028	0.280 ± 0.031
3.50 ^h	160	20	-4.438 ± 0.291	0.570 ± 0.048	0.234 ± 0.037
3.50 ^c	220	20	-4.108 ± 0.281	0.500 ± 0.053	0.180 ± 0.040
3.55 ^c	577	80	-3.778 ± 0.407	0.446 ± 0.091	0.150 ± 0.060
3.55 ^h	400	20	-3.920 ± 0.342	0.483 ± 0.070	0.170 ± 0.049
3.60 ^c	620	40	-3.118 ± 0.293	0.288 ± 0.085	0.069 ± 0.038
3.60 ^h	60	60	-2.650 ± 0.161	0.101 ± 0.022	0.014 ± 0.016
3.65 ^c	120	40	-2.710 ± 0.178	0.186 ± 0.044	0.027 ± 0.019
3.65 ^h	140	20	-2.640 ± 0.186	0.130 ± 0.060	0.013 ± 0.019
3.70 ^c	80	20	-2.517 ± 0.161	0.116 ± 0.048	0.015 ± 0.019
3.70 ^h	100	20	-2.516 ± 0.150	0.092 ± 0.027	0.005 ± 0.016
3.80 ^c	140	20	-2.384 ± 0.157	0.099 ± 0.035	0.009 ± 0.016
4.00 ^c	140	40	-2.041 ± 0.158	0.089 ± 0.035	0.007 ± 0.017
4.20 ^c	20	40	-1.735 ± 0.136	0.060 ± 0.018	0.006 ± 0.013
4.40 ^c	20	40	-1.496 ± 0.152	0.073 ± 0.024	0.008 ± 0.013
4.60 ^c	20	40	-1.237 ± 0.153	0.054 ± 0.019	0.007 ± 0.014

Runs marked ^h and ^c refer to heating and cooling runs respectively.

system spends time in the isotropic and ordered phase, as we have seen in the evolution diagrams of Fig. 2. In Fig. 5 we see that this is quite apparent when comparing energy histograms at various temperatures around the NI transition.

The histograms $P(U^*)$ represents the frequency of occurrence of a certain energy value during the simulation. We have considered all occurrences of the observable (the energy in Fig. 5) both for the cooling and heating sequences. Near the transition this means that up to 10^6 cycles contribute to the histograms. As we see, the peaks are extremely

sharp and the deviation from gaussian shape quite small at low temperatures. On the other hand the histograms become extremely non-gaussian and start to show a two-overlapping-peak behaviour near the isotropic transition. Such a behaviour has been observed³ for the Lebwohl-Lasher model where a much larger sample size allows examining the neighbourhood of the transition in finer detail. For instance, an estimate for the temperature of divergence of the pretransitional effects could be given in that case, while we have not attempted this here. In Fig. 6 we show the temperature variation of k_2 , k_3 and k_4 , the second, third and fourth cumulants

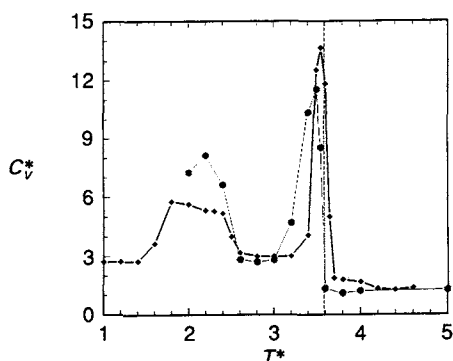


Fig. 4 The dimensionless specific heat C_v^* plotted against scaled temperature T^* for the $N = 1000$ (\blacklozenge) and $N = 512$ (\bullet) systems

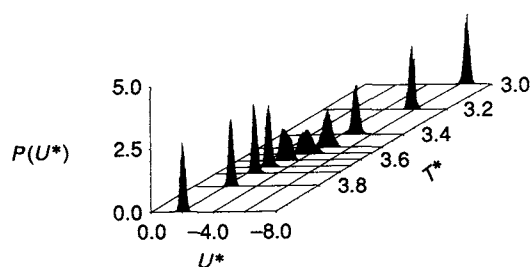


Fig. 5 Histograms $P(U^*)$ of the scaled energy values U^* occurring during the simulation runs for the $N = 1000$ system at various scaled temperatures T^* around the nematic-isotropic transition. All histograms have been normalized to the same unit area and comprise both the cooling and heating sequences.

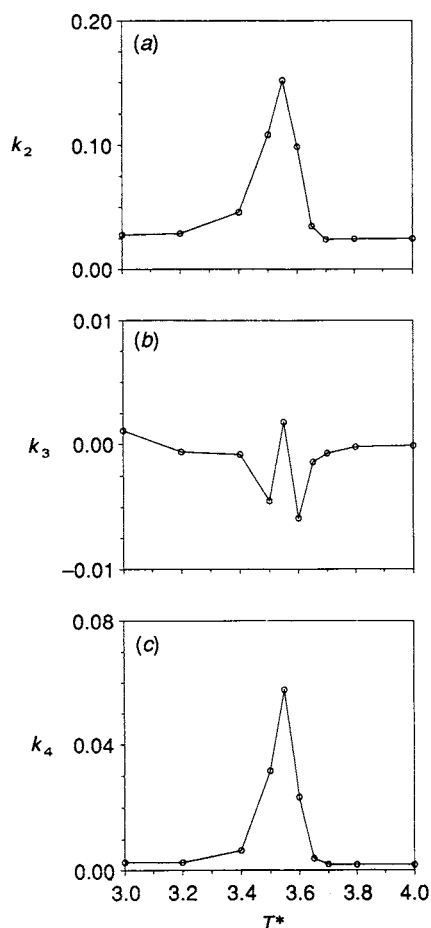


Fig. 6 Plot of the second (a), third (b) and fourth (c) cumulants of $P(U^*)$ vs. T^* around the nematic-isotropic transition

of $P(U^*)$. We recall that $k_2 = m_2$, $k_3 = m_3$ and $k_4 = m_4 - 3m_2^2$, where the n th central moment of U^* , m_n^U , is

$$m_n^U = \sum_k (U_k^* - \langle U^* \rangle)^n P_k(U^*) \quad (8)$$

and P_k is the population of the histogram at bucket k , normalized so that $m_0^U = 1$. We notice that the width of the peaks, given by k_2 , is very small except near the transition, where an increase of an order of magnitude is apparent. The gaussian character of the peaks outside the transition region is confirmed by the very small fourth cumulant (expected to be zero for a true gaussian). Notice that the skewness, as signalled by k_3 , is always small, and that it changes sign between $T^* = 3.55$ and $T^* = 3.60$. The rather large fluctuations in k_3 depend probably on the still limited sample size.

We can estimate the transition temperature from the change of sign of k_3 and obtain $T_{NI}^* \approx 3.57$. The energy histograms also allow estimation of the entropy of transition from the relation $\Delta S_{NI}^* = \Delta U_{NI}^*/T_{NI}^*$. We find, even though in a rather approximate way, $\Delta S_{NI}^* \approx 0.2 \pm 0.1$.

2.2 Structure of the Phases

Having located the temperatures where the heat capacity presents anomalies it is now worth looking more closely at the molecular organization in the different regions. We start by looking at configuration snapshots at six temperatures (see Plate 1). The molecules are represented with ellipsoids and their orientation is given by a colour code as we have previously done for lattice models³¹ (see palette in Plate 1). Here

we find the director of each configuration and we rotate the sample so as to bring the director along the laboratory z axis. The sample is then viewed from an observation point placed at polar angles $\theta = 27.5^\circ$ and $\phi = 25^\circ$. The perspective rendering, illumination and shading is done on a HP720 using the Phong algorithm^{32a,b} and the configurations are further assembled as shown in Plates 1 and 2 using the San Diego Supercomputer Centre 'Image Tools'.^{32c} To facilitate observation the particles are shrunk by a scaling factor of 0.8.

On examining the configurations the change in organization is quite apparent. For the temperatures in the region of the first C_V^* peak (here $T^* = 1.8$ and $T^* = 2.0$) the system has a well ordered near crystalline or smectic structure, with the molecular axis perpendicular on average to the layers, thus with smectic A or B character. The layered structure is lost in the $T^* = 2.80$ and $T^* = 3.50$ snapshots, where the structure clearly appears to be nematic. The orientational disorder, here signalled by an increase in the number of the differently coloured molecules (which in turn compete to orientations with significant misalignment from the director) increases with temperature as expected. At $T^* = 3.8$ the system has become isotropic and all orientations, here all colours of the palette, are present. It is interesting to see that even above T_{NI}^* we have groups of neighbouring molecules of the same colour and thus with similar orientations. This provides an immediate visualization of the existing short-range order or local domains. Some pretransitional order remains even at the highest temperature shown, $T^* = 4.0$, *ca.* 10% above the transition.

In Plate 2 we show snapshots of the same configurations at the six different temperatures from a viewpoint perpendicular to the director. In this transversal view six layers are clearly visible at $T^* = 1.80$ and 2.00 . It should be remembered that a shrinking factor of 0.8 is applied to the particles to facilitate viewing of the layers that are actually somewhat interdigitated, without the slight interlayer space apparent in the figure.

It is clear that this pictorial representation, although useful, has to be complemented by more quantitative numerical observables. Here we have calculated a variety of them. First we examine the distribution of intermolecular vectors. This can be introduced starting from the general two particle distribution $P^{(2)}(\mathbf{r}_1, \omega_1, \mathbf{r}_2, \omega_2)$ giving the probability of finding any two particles at $(\mathbf{r}_1, \omega_1, \mathbf{r}_2, \omega_2)$. This pair distribution will reduce for large intermolecular separations to the product of the singlet distributions for the two molecules: $P(\mathbf{r}_1, \omega_1)$, $P(\mathbf{r}_2, \omega_2)$.³³ At short and intermediate distances the position-orientation of the two molecules are interdependent. A pair correlation function is defined³³ as

$$g^{(2)}(\mathbf{r}_1, \omega_1; \mathbf{r}_2, \omega_2) = \frac{P^{(2)}(\mathbf{r}_1, \omega_1, \mathbf{r}_2, \omega_2)}{P(\mathbf{r}_1, \omega_1)P(\mathbf{r}_2, \omega_2)} \quad (9)$$

so that $g^{(2)}(\mathbf{r}_1, \omega_1, \mathbf{r}_2, \omega_2)$ goes to one in the limit of large intermolecular separations. Then a distribution of the intermolecular vector around a molecule taken as origin is introduced by integration over the orientations of the two particles and the position of the first particle:

$$g(r, \omega_r) = \frac{\int d\mathbf{r}_1 d\omega_1 d\omega_2 g^{(2)}(\mathbf{r}_1, \omega_1; \mathbf{r}_1 + \mathbf{r}, \omega_2)}{\int d\mathbf{r}_1 d\omega_1 d\omega_2} \quad (10)$$

This quantity gives the probability of finding a particle at a certain distance r from a particle chosen as origin when their intermolecular vector has orientation $\omega_r = (\alpha_r, \beta_r)$. Notice that the systems considered here are at most uniaxial, so if we consider orientations defined with respect to a laboratory

system with z axis parallel to the director we do not need to consider the angle α_r and the intermolecular vector distribution reduces to $g(r) = g(r, \beta_r)/2\pi$. The significance of this distribution will become clearer if we look at Fig. 7 where we show results for this quantity, reported as $g(r^*, \cos \beta_r)$, at the six different temperatures considered in Plates 1 and 2.

The three-dimensional representation shows at once that the radial distribution is far from isotropic even in the nematic phase, an assumption often, even though not always, made by simple mean field theory.^{34,35} In addition the function changes quite significantly with temperature. The very low temperature one ($T^* = 1.8$) shows that as we move from a molecule along the z laboratory axis ($\cos \beta_r = 1$) a second molecule is found slightly below σ_e . However if we move transversally to the director ($\cos \beta_r = 0$) very sharp, well defined peaks appear. At least six orders of peaks occur, indicating a high degree of structure in the layer. A more careful look at the double structure of the second peak betrays this structure for an hexagonal ordering, as expected in a smectic B or crystalline layer structure. In particular, as in a triangular lattice in the layer, we have first the sharp nearest-neighbours peak, then a double peak with similar intensities around $r^* = 2$, another double peak with 2 : 1 intensity factor between $r^* = 2.6$ and 3.0. These would appear at $r^* = 1.73$ and 2 and at 2.646 and 3 for the perfect triangular lattice. At $T^* = 2.0$ the structure is quite similar, although less resolved. We still have order in the layer but the characteristic features of hexagonal ordering are not evident. We are not able to ascertain any sharp transition between these different low-temperature configurations. We recall that the specific heat curve in Fig. 4 was also not so helpful in this respect, showing essentially a broad hump. The ordering inside the layer

decreases significantly on increasing the temperature and disappears, except for a couple of shells, in the nematic. At $T^* = 2.8$ the layer organization is lost, even if some short-range translational order remains. The further increase in temperature to $T^* = 3.5$ only shows a further reduction in transversal order. As we move to the isotropic phase the structure is flat and essentially the same in all directions.

The ordered structure of the $\mu = 2, \nu = 1$ model at $\rho^* = 0.30$ bordering with the isotropic is not very well characterized in ref. 14 and was assigned to a nematic in ref. 16. To examine the nature of the molecular organization transforming to the isotropic phase we have also calculated a few additional quantities. One is the pair correlation along the director, *i.e.* along the z direction. This gives the probability of finding a second molecule with a vertical displacement of z along the director from one taken as origin.

$$g(z) = \frac{\int dr r^2 d\beta_r \sin \beta_r \delta(r \cos \beta_r - z) g(r, \beta_r)}{\int dr r^2 d\beta_r \sin \beta_r \delta(r \cos \beta_r - z)} \quad (11)$$

This quantity is plotted in Fig. 8 in terms of scaled displacement z^* , $z^* \equiv z/\sigma_s$ for a set of temperatures around the low- and the high-temperature anomaly in the heat capacity. Notice that the function starts from a non-zero value, corresponding to the probability of finding other molecules with the same elevation as that at the origin, as is the case when a layered structure exists. We see clearly the change from the regular periodic pattern of the smectic to the flat distribution of the nematic structure around $T^* = 2.4$. We also see, from the curve at $T^* = 3.5$ that our $\mu = 1, \nu = 3$ system is defi-

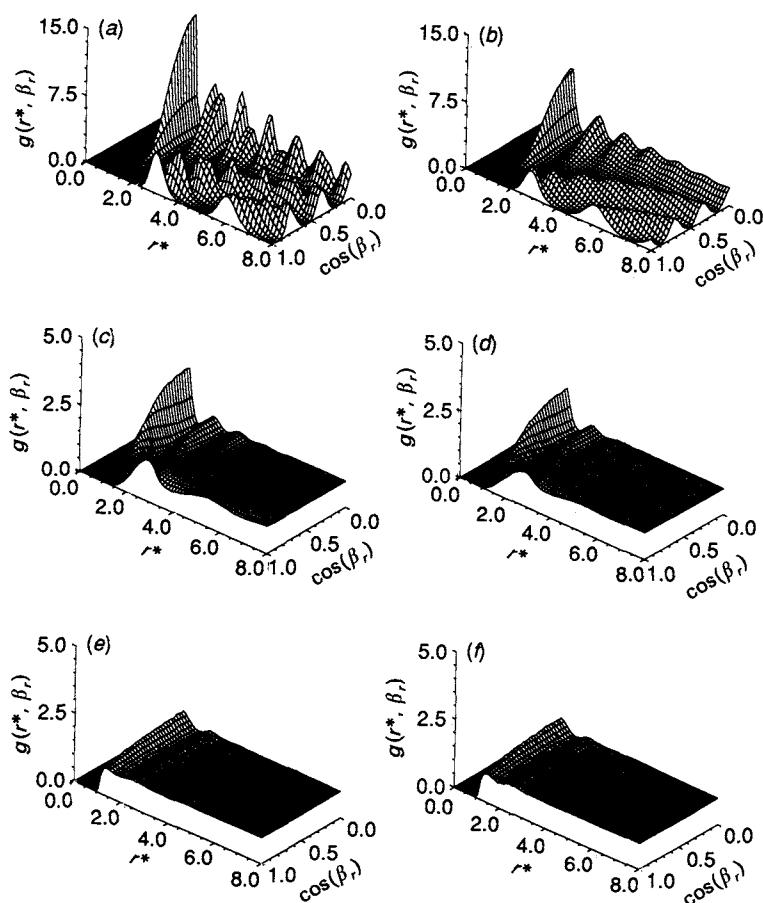


Fig. 7 The intermolecular vector distribution $g(r^*, \beta_r)$ as a function of scaled separation r^* and of the angle β_r between intermolecular vector and director for the $N = 1000$ system. The scaled temperatures correspond to those of the configurations in Plate 1.

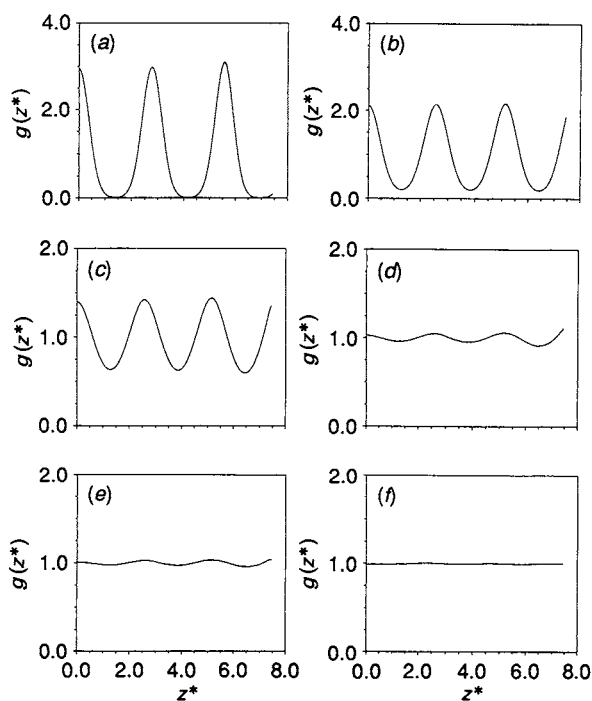


Fig. 8 Pair correlation function along the director, $g(z^*)$, for the $N = 1000$ system at various scaled temperatures in the crystalline, smectic: $T^* = (a) 1.80^h, (b) 2.00^h, (c) 2.30^h$ and nematic: $T^* = (d) 2.40^h, (e) 2.80^h, (f) 3.50^h$ phase

nitely nematic rather than smectic before it becomes isotropic.

It is convenient to expand $g(r, \beta_r)$ as

$$g(r, \beta_r) = g_0(r) \sum_L (2L + 1) g_L^+(r) P_L(\cos \beta_r) \quad (12)$$

where $g_0(r)$ is the standard radial distribution

$$g_0(r) = \frac{1}{2} \int d\beta_r \sin \beta_r g(r, \beta_r) \quad (13)$$

The set of quantities $g_L^+(r)$ associated with the intermolecular vector correlation function represent a sort of order parameters.^{17,35}

$$g_L^+(r) = \frac{1}{2g_0(r)} \int d\beta_r \sin \beta_r g(r, \beta_r) P_L(\cos \beta_r) \quad (14a)$$

$$= \langle P_L(\cos \beta_r) \rangle_r \quad (14b)$$

In practice $g_0^+(r) = 1$ and $g_2^+(r)$ represents the first non-vanishing anisotropic term. In Fig. 9(a) and (b) we report a set of these parameters for some selected temperatures.

The radial distribution $g_0(r^*)$ shows once more, although in a different and perhaps more familiar way, the loss of long-range positional order as the temperature increases. From this point of view the smectic (and of course crystalline) phases differ from the nematic more than the nematic differs from the isotropic phase. Indeed if we compare $g_0(r^*)$ for two temperatures relatively near to T_{NI}^* on the ordered and disordered sides [namely $T^* = 3.5$ and 3.65 in Fig. 9(a)] we see a great similarity, with only some quantitative difference. This is in agreement with a conjecture of Luckhurst and Zannoni³⁶ which made the hypothesis of a similar short-range structure on the two sides of the transition as a cause for the small entropy jump at the nematic-isotropic transition.

The second-rank angular anisotropy of the intermolecular vector distribution, $g_2^+(r^*)$, plotted in Fig. 9(b) shows that the

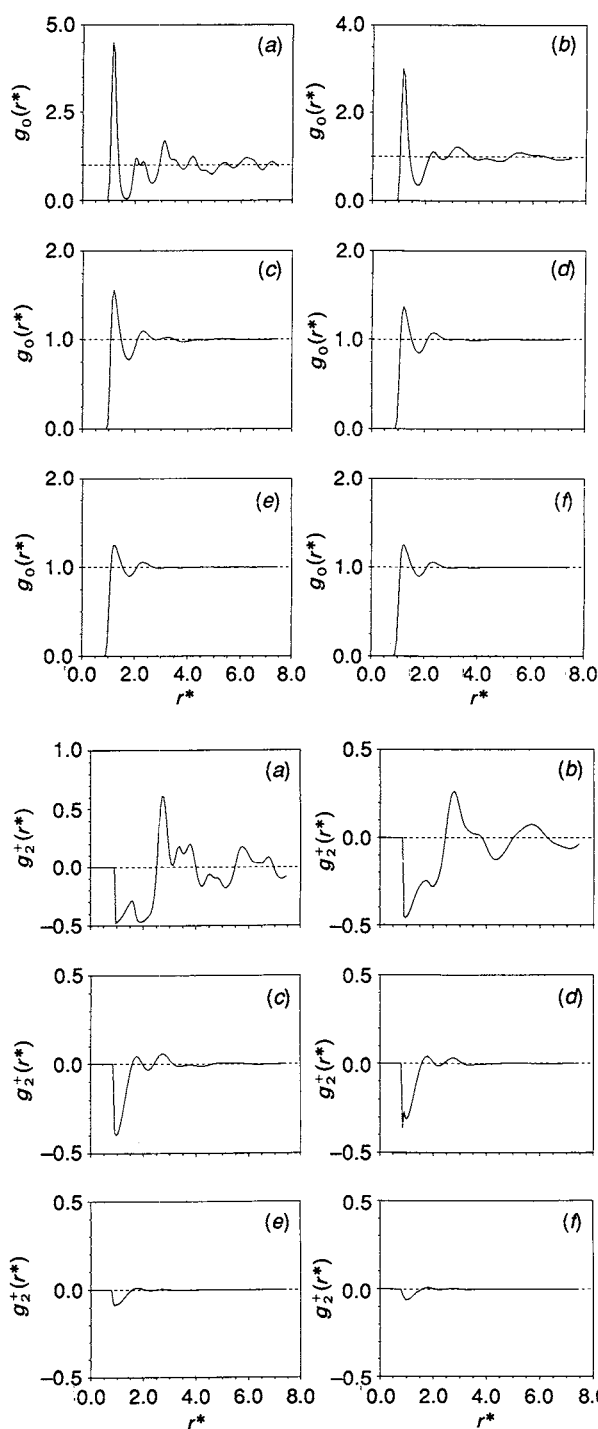


Fig. 9 The radial distribution function $g_0(r^*)$ and its second-rank anisotropy $g_2^+(r^*)$ at various scaled temperatures in the crystalline, smectic: $T^* = (a) 1.80^h, (b) 2.00^h$, nematic: $T^* = (c) 2.80^h, (d) 3.50^h$ and isotropic: $T^* = (e) 3.65^\circ, (f) 3.80^\circ$ phase

nearest-neighbour vector is essentially perpendicular to the director both in the smectic and the nematic phases. In fact $g_2^+(r^*) = \langle P_2(\cos \beta_r) \rangle_r$ is negative (and thus on average $\beta_r > 54.7^\circ$ even at $T^* = 3.5$). In the isotropic phase we still have short-range clusters of molecules, as we have seen from the snapshots and from $g_0(r^*)$. Moreover the clusters are essentially randomly oriented with respect to the instantaneous preferred orientation and thus the peak, although still negative, is very small. We also see that in the nematic (and of course in the isotropic) phase the anisotropy of the intermolecular vector distribution goes to zero very quickly. Once more this seems to be in agreement with ref. 36 and shows

the importance of looking at the structural data produced by the simulations in a number of ways.

2.3 Orientational Order Parameters

Molecular orientational order parameters of second and fourth rank: $\langle P_2 \rangle$ and $\langle P_4 \rangle$, have been determined. In particular we have calculated and diagonalized the laboratory frame tensor $\langle \mathbf{A}^L \rangle_s$ with elements³

$$\langle A_{ab}^L \rangle_s = \langle u_a u_b \rangle_s \quad (15a)$$

$$= \frac{1}{N} \sum_{i=1}^N [(u_i)_a (u_i)_b] \quad (15b)$$

where $(u_i)_a$ are the components of the unit vector u_i giving the orientation of the axis of molecule i and $\langle \dots \rangle_s$ indicates an average over the sample configuration. In practice the calculation is done every 20 cycles, to reduce the unavoidable correlation between nearby configurations in the Monte Carlo chain while avoiding a waste of computer time.

The second-rank order parameter for the J th configuration is obtained from the largest eigenvalue of the ordering matrix $\langle \mathbf{Q}^L \rangle_s \equiv \langle \mathbf{A}^L \rangle_s - (1/3)\mathbf{I}$, i.e. λ_{\max}^J and the average $\langle P_2 \rangle$ is produced from the overall configurational average of these λ_{\max}^J as $\langle P_2 \rangle = 3\lambda_{\max}^J/2$. The errors quoted in Tables 2 and 3 are calculated as the corresponding standard deviations. We have also calculated for the first time for the GB model the fourth-rank order parameter $\langle P_4 \rangle$. This was done from the sample average of a fourth-rank tensor F , constructed as direct product of \mathbf{A} , transformed to the director frame of the configuration as determined by the eigenvector matrix U of $\langle \mathbf{Q} \rangle_s$.³ More explicitly the director d is obtained as the eigenvector corresponding to λ_{\max} and the fourth-rank order parameter $\langle P_4 \rangle$ can be obtained from the director frame tensor element

$$\langle F_{zzzz}^D \rangle_s = \langle \cos^4 \beta \rangle_s \quad (16a)$$

$$= \sum_{a,b,c,d} U_{az} U_{bz} U_{cz} U_{dz} \langle F_{abcd}^L \rangle_s \quad (16b)$$

with $\langle F_{abcd}^L \rangle_s = \langle u_a u_b u_c u_d \rangle_s$ and $\cos \beta \equiv u \cdot d$

$$\langle P_4 \rangle_s = \frac{35}{8} \langle \cos^4 \beta \rangle_s - \frac{39}{8} \langle \cos^2 \beta \rangle_s + \frac{3}{8} \quad (17)$$

The average fourth-rank order parameters reported in Table 3 are then obtained as configurational averages.

In Fig. 10 we show $\langle P_2 \rangle$ and $\langle P_4 \rangle$ as a function of temperature for the heating and cooling stages of the $N = 1000$

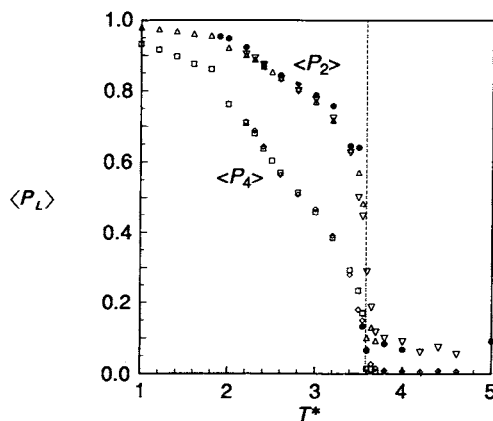


Fig. 10 Orientational order parameters as a function of scaled temperature, (a)–(f) as Fig. 9. We show results for $\langle P_2 \rangle$, $\langle P_4 \rangle$ of the $N = 1000$ system in a cooling (∇ , \diamond) and heating (\triangle , \square) sequences as well as results for $N = 512$ (\bullet). The vertical dashed line indicates the nematic-isotropic transition.

system and for the $N = 512$ system (filled circles). We see an essentially continuous behaviour for these parameters even at the smectic–nematic transformation with a very sharp decrease at the nematic–isotropic transition. The average value of $\langle P_2 \rangle$ at the transition is quite large, being above 0.4.

Remembering the large fluctuations at the transition observed earlier for the energy, it is important to examine, also for the order parameters, the distribution of values obtained from the simulations. In Fig. 11 we show histograms of $\langle P_2 \rangle$ around the nematic–isotropic transition for the $N = 1000$ system. We see that $\langle P_2 \rangle$ has a very broad distribution at $T^* = 3.55$ and that the largest value of $\langle P_2 \rangle$ to which a significant peak competes is about 0.45, that we take as our estimate of $\langle P_2 \rangle_{\text{NI}}$.

Such a large change in $\langle P_2 \rangle$ is rather unusual for computer simulations and seems higher than that found for the other Gay–Berne system studied so far.¹⁶ Part of the problem may simply reside in the sharp decrease of $\langle P_2 \rangle$ coupled with an uncertain location of the nematic–isotropic transition.

Turning to the fourth-rank order parameter, also reported in Fig. 10, we see that it is always positive and that it decreases with temperature as expected. The temperature variation, although broadly similar, does not have the same curvature as that of $\langle P_2 \rangle$ and the jump at the transition is very small. We estimate from the histograms of $\langle P_4 \rangle$ (not shown) $\langle P_4 \rangle_{\text{NI}} \approx 0.12$.

The $\langle P_4 \rangle$ vs. $\langle P_2 \rangle$ curve is universal as long as the singlet distribution has an exponent or potential of mean torque with second Legendre polynomial character.³ This curve is represented as the continuous line in Fig. 12. The heating and cooling results shown in Fig. 12 are slightly but significantly above this curve. By comparison the $\langle P_4 \rangle$ vs. $\langle P_2 \rangle$ results for the Lebwohl–Lasher model lay below the same universal curve.³

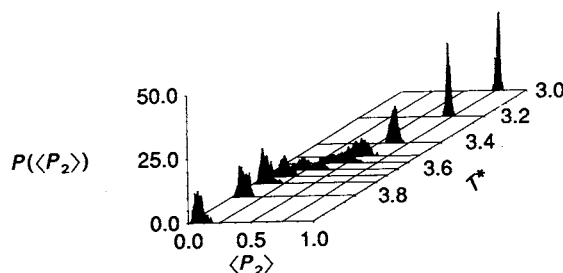


Fig. 11 Histograms $P(\langle P_2 \rangle)$ of the frequency of occurrence of $\langle P_2 \rangle$ values occurring during the simulation runs for the $N = 1000$ system at various scaled temperatures around the nematic–isotropic transition. All histograms are normalized to the same unit area and are cumulated for both the cooling and heating sequences.

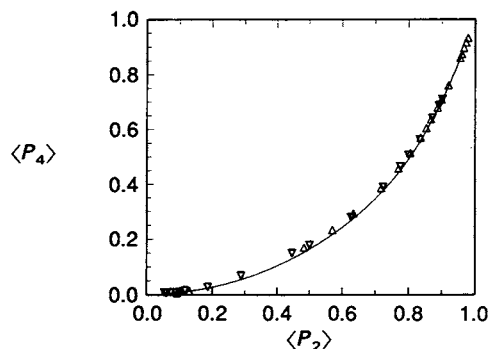


Fig. 12 $\langle P_4 \rangle$ vs. $\langle P_2 \rangle$ for $N = 1000$ system in the heating (\triangle) and cooling (∇) runs compared with the Maier–Saupe prediction (continuous line)

We now wish to turn to a comparison of our results with those for other GB models. In particular an important question we should ask is: Given a certain molecular shape and shape anisotropy, what is the role of the strength of interaction parameters, in particular of the exponents μ and ν ? Until recently, very little consideration has been given to the adjustable part of the potential. Even in the very extensive study of the GB potential by de Miguel *et al.*^{14,15} there was no attempt to utilize values of μ and ν different to those determined by Gay and Berne. In a slightly different formulation of the GB potential due to Gupta *et al.*³⁷ the μ and ν parameters have been fixed to one and the potential has been tuned otherwise. Thus is interesting to compare our results with those available for the $\mu = 2, \nu = 1$ case. We notice at first some qualitative differences. At a density of $\rho^* = 0.30$ the work of de Miguel *et al.*¹⁴ with the original GB potential hints at the possibility of an isotropic–smectic B transition, while we have confidently demonstrated the existence of a relatively wide-range nematic phase. A nematic was found also in ref. 16. Moreover, Fig. 4 and 12 show a strong transition while other Gay–Berne simulation studies predict weaker NI transitions. In particular Emsley *et al.*¹⁶ have studied the $\mu = 2, \nu = 1$ model at $\rho^* = 0.3, 0.32, 0.35$. They have found very large temperature shifts for this relatively large density variation. For instance the nematic–isotropic transition was found¹⁶ to go from 0.94 to 1.51 and 3.29 for the three densities. In all the systems the transition was, however, found to be rather continuous and the second-rank order parameter well approximated by the expression:

$$\langle P_2 \rangle = (1 - \langle P_2 \rangle_1) \left(1 - \frac{T^*}{T_{NI}^*} \right)^\beta + \langle P_2 \rangle_1 \quad (18)$$

where $\langle P_2 \rangle_1$ is the residual order parameter in the isotropic phase that is different from zero in a finite system and was taken to be 0.1 in the $N = 256$ system used in ref. 16. For $\rho^* = 0.30$ the exponent β was found to be 0.37 and this curve is plotted in Fig. 13 as the dashed line. A similar fit on our data, using $\langle P_2 \rangle_1 = 0.1$ and $T_{NI}^* = 3.57$ gave $\beta = 0.17$ *i.e.* roughly half of that in ref. 16. An expression essentially analogous to eqn. (18) was used by Leenhouts *et al.*³⁸ to fit their experimental results for the diamagnetic susceptibility anisotropy in a series of 12 Schiff's base nematics which include the popular mesogens *n*-(4-methoxybenzylidene)-4'-*n*-butylaniline (MBBA), with $\beta = 0.174$, and anisylidene-*p*-aminophenylacetate (APAPA), with $\beta = 0.185$. In that case an exponent $\beta = 0.17$ – 0.21 was found to fit all their compounds.

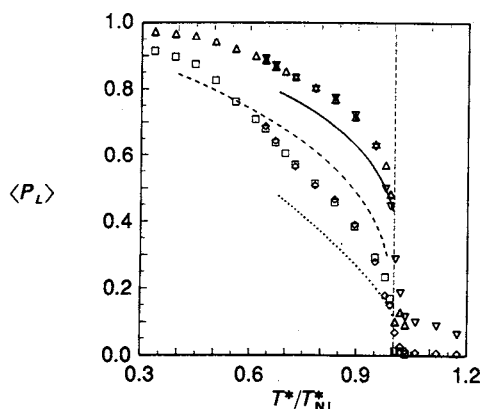


Fig. 13 Orientational order parameters as a function of reduced temperature T^*/T_{NI}^* . We show results for $\langle P_2 \rangle, \langle P_4 \rangle$ of the $N = 1000$ system in a cooling (∇, \diamond) and heating (Δ, \square) sequence, together with Maier–Saupe curves (continuous and dotted lines for $\langle P_2 \rangle$ and $\langle P_4 \rangle$). We also show $\langle P_2 \rangle$ as obtained for the $\mu = 2, \nu = 1$ model¹⁶ (dashed line). The vertical dashed line indicates the nematic–isotropic transition.

A similar fitting of birefringence data for 4-*n*-pentyl-4'-cyano-biphenyl (5CB) by Wu and Cox gave an exponent $\beta = 0.172$ with again values in the range $\beta = 0.17$ – 0.22 for other compounds.³⁹ It is comforting to see that the present choice of model parameters seems to give one of the fundamental properties for liquid crystals: the temperature variation of the order parameter, in agreement with the behaviour of many real systems.

In Fig. 13 we also show $\langle P_2 \rangle$ and $\langle P_4 \rangle$ vs. reduced temperature T^*/T_{NI}^* for the heating and cooling sequences and the Maier–Saupe theory predictions for $\langle P_2 \rangle$ (continuous line) and $\langle P_4 \rangle$ (dotted line).

In summary it seems then that changing μ from 2 to 1 and ν from 1 to 3, while not altering the shape and well-depth anisotropies, has a rather dramatic effect on the stability of the nematic phase. The reason for this may be traced back from the potential plot in Fig. 1. Although the relative well depths for the end-to-end and side-by-side configurations are unaffected we see that the perpendicular 'T' arrangement is destabilized with respect to the former two. Since this configuration arises easily in the isotropic phase, but is not likely to be favoured in the nematic phase we might expect a greater propensity for mesophase formation.

3. Conclusions

We have performed a detailed study of the temperature dependence and of the nematic–isotropic phase transition in two Gay–Berne model systems composed of 512 and of 1000 particles. We have looked at the character of the nematic–isotropic transition and we have found it necessary to perform very lengthy runs to be able to study this. We have found a relatively strong transition, as compared with the published results for the standard ($\mu = 2, \nu = 1$) potential. We have found that $\langle P_2 \rangle$ is larger than that expected for a simple Maier–Saupe model and that $\langle P_4 \rangle$ is also slightly higher than that predicted for a pure P_2 effective potential. We have found practically no hysteresis and that the results for heating and cooling runs are essentially superimposable.

A comparison of our results for the $\mu = 1, \nu = 3$ model with those for the standard potential shows that the properties of these two GB fluids with the same size and shape factors but with different attractive interaction parameters can vary significantly. The temperature dependence of the order parameter for the present model is characterized by an exponent $\beta = 0.17$ very similar to that obtained experimentally^{38,39} for a wide range of compounds. Our results confirm the great potential of the GB potential for modelling liquid crystal behaviour and the usefulness of exploring the effects of changing the parameters in the model.

We are grateful to the Royal Society (London) and to CNR, Progetto Finalizzato 'Sistemi informatici e Calcolo Parallelo' (Rome), for postdoctoral fellowships to A.E. and R.B. respectively. We also thank MURST and CNR for support. The simulations described in this work were run on three HP720 RISC workstations and amount to well over 6000 h CPU time. We wish to thank Hewlett–Packard Ital. for their very helpful support. We have appreciated collaboration and discussions with P. F. Bini, S. Boschi (particularly on the graphic rendering of configurations), C. Chiccoli, P. Pasini and F. Semeria.

References

- 1 *Computer Simulation of Liquid Crystals*, ed. G. R. Luckhurst, NATO Advanced Research Workshop, Il Ciocco, 1991, Kluwer, Dordrecht, 1994, in the press.

- 2 P. A. Lebowitz and G. Lasher, *Phys. Rev. A*, 1972, **6**, 426.
- 3 U. Fabbri and C. Zannoni, *Mol. Phys.*, 1986, **58**, 763.
- 4 D. Frenkel, *Mol. Phys.*, 1987, **60**, 1.
- 5 D. Frenkel and B. M. Mulder, *Mol. Phys.*, 1985, **55**, 1171.
- 6 M. P. Allen, D. Frenkel and J. Talbot, *Comput. Phys. Rep.*, 1989, **9**, 301.
- 7 G. R. Luckhurst and S. Romano, *Proc. R. Soc. London, A*, 1980, **373**, 111.
- 8 B. J. Berne and P. Pechukas, *J. Chem. Phys.*, 1972, **56**, 4213.
- 9 J. Kushick and B. J. Berne, *J. Chem. Phys.*, 1976, **64**, 1362.
- 10 A. L. Tsykalo and A. D. Bagmet, *Mol. Cryst. Liquid Cryst.*, 1978, **46**, 111; *Czech. J. Phys. B*, 1978, **28**, 1113.
- 11 J. G. Gay and B. J. Berne, *J. Chem. Phys.*, 1981, **74**, 3316.
- 12 D. J. Adams, G. R. Luckhurst and R. W. Phippen, *Mol. Phys.*, 1987, **61**, 1575.
- 13 G. R. Luckhurst, R. A. Stephens and R. W. Phippen, *Liq. Cryst.*, 1990, **8**, 451.
- 14 M. K. Chalam, K. E. Gubbins, E. de Miguel and L. F. Rull, *Mol. Simul.*, 1991, **7**, 357.
- 15 E. de Miguel, L. F. Rull, M. K. Chalam, K. E. Gubbins and F. van Swol, *Mol. Phys.*, 1991, **72**, 593.
- 16 J. W. Emsley, G. R. Luckhurst, W. E. Palke and D. J. Tildesley, *Liq. Cryst.*, 1992, **11**, 519.
- 17 A. P. J. Emerson, R. Hashim and G. R. Luckhurst, *Mol. Phys.*, 1992, **76**, 241.
- 18 G. R. Luckhurst, *Liq. Cryst. Today*, 1993, **3**, 3.
- 19 E. Egberts and H. J. C. Berendsen, *J. Chem. Phys.*, 1988, **89**, 3718.
- 20 S. J. Picken, W. F. van Gunsteren, P. Th. van Duijnen and W. H. de Jeu, *Liq. Cryst.*, 1989, **6**, 357.
- 21 M. R. Wilson and M. P. Allen, *Mol. Cryst. Liq. Cryst.*, 1991, **198**, 465; *Liq. Cryst.*, 1992, **12**, 157.
- 22 A. J. Stone, *The Molecular Physics of Liquid Crystals*, ed. G. R. Luckhurst and G. W. Gray, Academic, 1979, ch. 2, p. 31.
- 23 G. R. Luckhurst, *J. Chem. Soc., Faraday Trans. 2*, 1988, **84**, 961.
- 24 Z. Zhang and O. Mouritsen, *Phys. Rev. Lett.*, 1992, **69**, 2803.
- 25 C. Chiccoli, P. Pasini, F. Semeria and C. Zannoni, *Phys. Lett. A*, 1990, **150**, 311.
- 26 F. Biscarini, C. Chiccoli, P. Pasini and C. Zannoni, *Mol. Phys.*, 1991, **73**, 439.
- 27 A. P. J. Emerson, C. Chiccoli, P. Pasini, F. Semeria and C. Zannoni, presented at the 14th ILCC, Pisa (H-P19), 1992.
- 28 J. A. Barker and R. O. Watts, *Chem. Phys. Lett.*, 1969, **3**, 144.
- 29 M. P. Allen and D. J. Tildesley, *Computer Simulation of Liquids*, Clarendon Press, Oxford, 1987.
- 30 C. Zannoni, *The Molecular Physics of Liquid Crystals*, ed. G. R. Luckhurst and G. W. Gray, Academic, 1979, ch. 9, p. 191.
- 31 C. Chiccoli, P. Pasini, F. Semeria and C. Zannoni, *Int. J. Mod. Phys. C*, 1992, **3**, 1209.
- 32 (a) B. T. Phong, *Comm. ACM*, 1975, **18**, 311; (b) D. F. Rogers, *Procedural Elements for Computer Graphics*, McGraw-Hill, Singapore, 1985; (c) San Diego Supercomputer Centre, 'Image Tools', 1992, version 2.1.
- 33 C. Zannoni, *The Molecular Physics of Liquid Crystals*, ed. G. R. Luckhurst and G. W. Gray, Academic, 1979, ch. 3, p. 51.
- 34 G. R. Luckhurst, *The Molecular Physics of Liquid Crystals*, ed. G. R. Luckhurst and G. W. Gray, Academic, 1979, ch. 4, p. 85.
- 35 R. L. Humphries, P. G. James and G. R. Luckhurst, *J. Chem. Soc., Faraday Trans. 2*, 1972, **68**, 1031.
- 36 G. R. Luckhurst and C. Zannoni, *Nature (London)*, 1977, **267**, 412.
- 37 S. Gupta, W. B. Sediawan and E. McLaughlin, *Mol. Phys.*, 1988, **65**, 961.
- 38 F. Leenhouts, W. H. de Jeu and A. J. Dekker, *J. Phys. (Paris)*, 1979, **40**, 989.
- 39 S. T. Wu and R. J. Cox, *J. Appl. Phys.*, 1988, **64**, 821.

Paper 3/03556E; Received 21st June, 1993

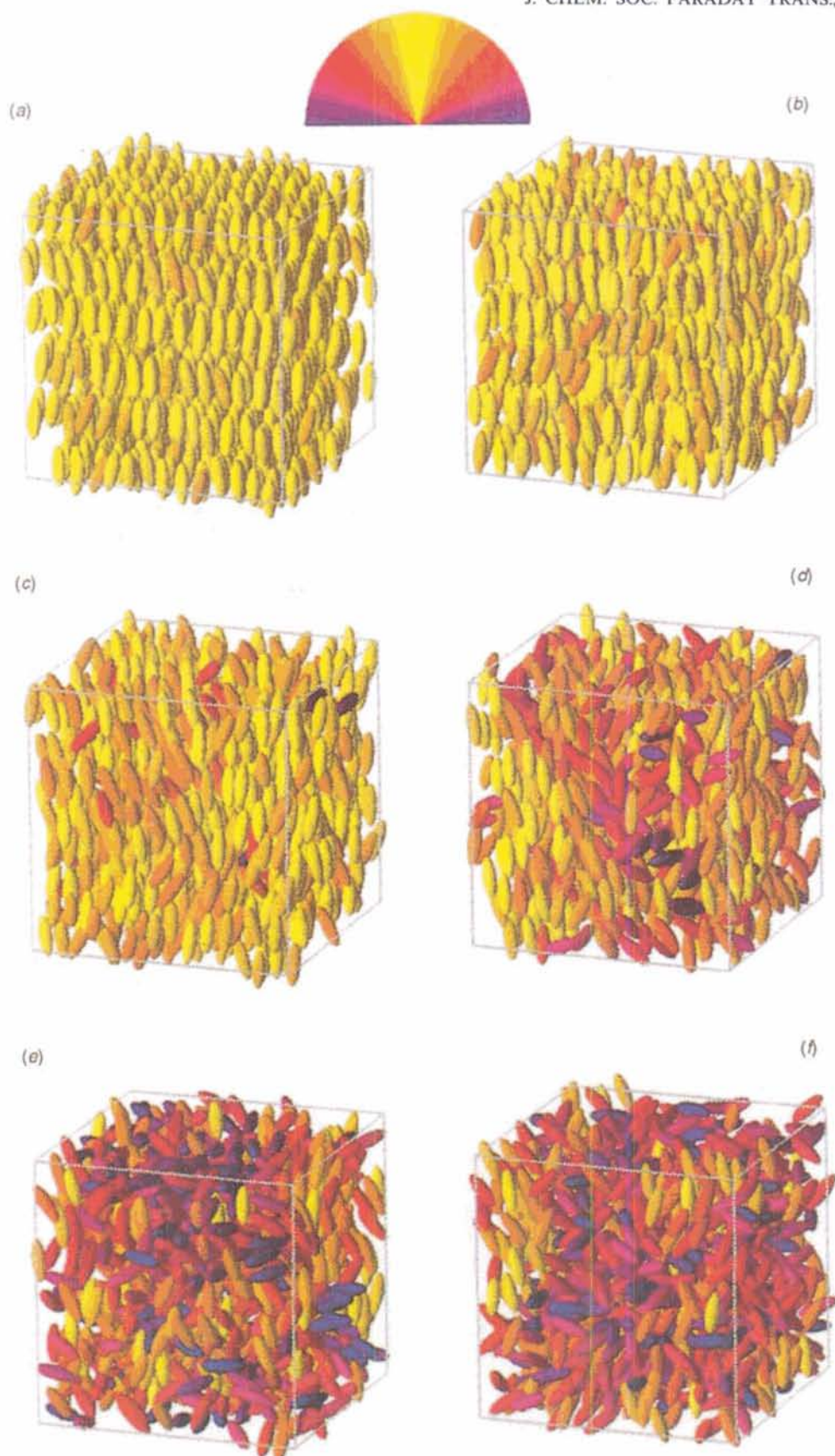


Plate 1 Snapshots of the Gay-Berne $N = 1000$ system at various scaled temperatures in the crystalline, smectic: $T^* = (a) 1.80^h$, $(b) 2.00^h$, nematic: $T^* = (c) 2.80^h$, $(d) 3.50^h$ and isotropic: $T^* = (e) 3.80^h$, $(f) 4.00^h$ phase. Molecular orientations with respect to the director are colour coded according to the palette shown. The sample is viewed from an observation point placed at polar angles $\theta = 27.5^\circ$ and $\phi = 25^\circ$.

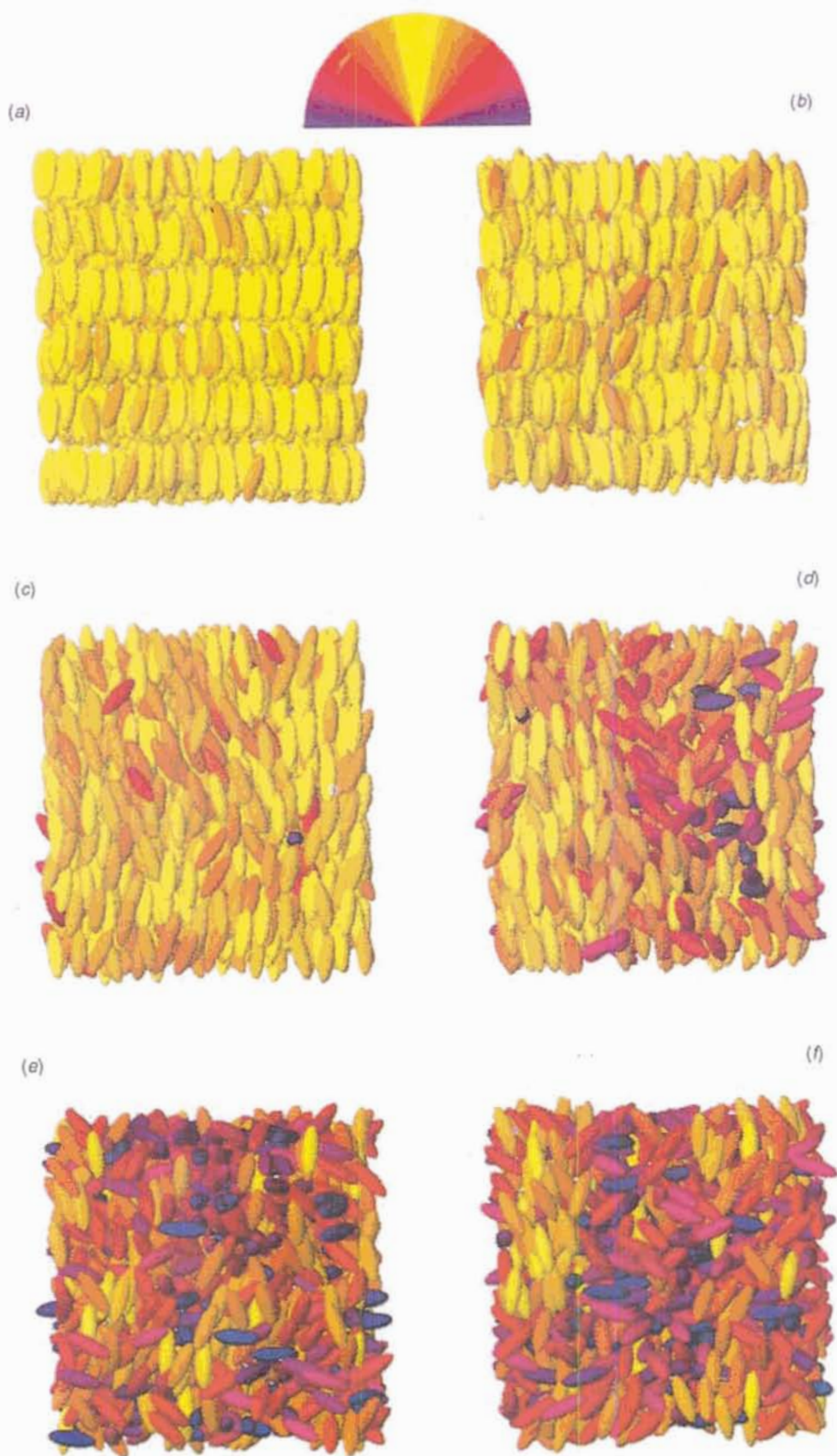


Plate 2 Transversal view snapshots of the Gay-Berne $N = 1000$ system at various scaled temperatures in the crystalline, smectic: $T^* = (a)$ 1.80^h , (b) 2.00^h , nematic: $T^* = (c)$ 2.80^h , (d) 3.50^h and isotropic: $T^* = (e)$ 3.80^e , (f) 4.00^e phase. Molecular orientations with respect to the director are colour coded according to the palette shown. The sample is viewed from an observation point placed at polar angles $\theta = 90^\circ$ and $\phi = 0^\circ$.